7-1-2017

Nonequilibrium polarization dynamics in antiferroelectrics

M. M. Vopson
University of Portsmouth

Xiaoli Tan
Iowa State University, xtan@iastate.edu

Nonequilibrium polarization dynamics in antiferroelectrics

Abstract
A nonequilibrium statistical domain nucleation model of polarization dynamics in less understood antiferroelectric systems is introduced. Predictions of the model have been successfully tested experimentally using an antiferroelectric Pb0.99Nb0.02[(Zr0.57Sn0.43) Ti-0.94(0.06)] O-0.98(3) polycrystalline ceramic. We determined the activation energy of the domain nucleation process for this particular antiferroelectric sample to be W-b = 1.07 eV and the critical volume of the polar nucleus V * = 98 x 10(-27)m(3), which corresponds to a linear length scale of 2.86 nm.

Disciplines
Condensed Matter Physics | Materials Science and Engineering

Comments
This article is published as Vopson, M. M., and Xiaoli Tan. "Nonequilibrium polarization dynamics in antiferroelectrics." *Physical Review B* 96, no. 1 (2017): 014104. doi: 10.1103/PhysRevB.96.014104. Posted with permission.

Nonequilibrium polarization dynamics in antiferroelectrics

M. M. Vopson[1,*,†] and X. Tan[2]
[1]*Faculty of Science, SEES, University of Portsmouth, Portsmouth PO1 3QL, United Kingdom*
[2]*Department of Materials Science and Engineering, Iowa State University, Ames, Iowa 50011, USA*
(Received 20 April 2017; published 7 July 2017)

A nonequilibrium statistical domain nucleation model of polarization dynamics in less understood antiferroelectric systems is introduced. Predictions of the model have been successfully tested experimentally using an antiferroelectric $Pb_{0.99}Nb_{0.02}[(Zr_{0.57}Sn_{0.43})_{0.94}Ti_{0.06}]_{0.98}O_3$ polycrystalline ceramic. We determined the activation energy of the domain nucleation process for this particular antiferroelectric sample to be $W_b = 1.07$ eV and the critical volume of the polar nucleus $V^* = 98 \times 10^{-27}\text{m}^3$, which corresponds to a linear length scale of 2.86 nm.

DOI: 10.1103/PhysRevB.96.014104

I. INTRODUCTION

Antiferroelectric materials were first predicted by Kittel in 1951 using Landau-Devonshire phenomenological theory [1] and shortly confirmed experimentally in $PbZrO_3$ ceramics [2,3]. Antiferroelectrics display a field induced transition from antipolar to polar dielectric, and they have interesting properties such as the double hysteresis loop and large strains associated with it. These unique properties make antiferroelectric materials very attractive for technological applications involving high-energy supercapacitors [4–8], electrocaloric cooling [9], actuators [10], photovoltaic effects [11], and many other interesting dielectric phenomena. Very recently, experimental evidence of a novel four-state nonvolatile memory effect in antiferroelectrics was reported [12]. A similar nonvolatile memory effect, but fundamentally different from the previously reported one, was published by Pešic *et al.* [13]. These simultaneous and independent studies concluded the possibility of utilizing antiferroelectric (AF) materials for nonvolatile random access memory (RAM) chips called AFRAM [14]. The AFRAM memories bring considerable improvements to ferroelectric RAM (FRAM) [15–19], while maintaining key features of FRAM such as low power consumption, ultrafast data access times, and read/write endurance of $>10^{12}$. These discoveries and proposed applications can be turned into commercial products only if the temperature, time, and electric field dependence of the polarization dynamics in antiferroelectrics are fully understood. Unfortunately, antiferroelectrics are complex systems and, despite major scientific advances [20–23], there is no clear understanding of their polarization dynamics.

The situation is rather different with ferroelectric materials, where the theories of polarization dynamics are well established and better understood. The wider consensus is that polarization reversal in ferroelectrics takes place via a nucleation of domains and the movement of domain walls, which subsequently expand and grow at the expense of the existing domains [24–29]. A simple phenomenological description of the polarization dynamics in ferroelectrics was given by Kolmogorov-Avrami-Ishibashi (KAI) domain nucleation-switching model [30–35] and subsequent variants of it [36–38]. The KAI model assumes that the application of an electric field generates nuclei of reversed polarization and that the polarization switching involves four steps: (i) nucleation of domains; (ii) rapid growth of nuclei along polarization direction; (iii) sidewise growth of the domains; and (iv) coalescence of the domains until full polarization reversal is completed. Despite being able to successfully describe polarization kinetics of ferroelectric single crystals [30] and some epitaxial thin films [39], the KAI model is very limited in applicability because of its failure to predict the relationship between the switching time to the applied electric field and temperature [36,40]. Various attempts to modify the KAI model in order to increase its applicability were made by assuming a distribution of relaxation times [37], a nucleation limited switching model [36], and a statistical time dependent depolarization field [38]. However, just as the KAI model, these variants still lack the full analytical inclusion of electric field, time, and temperature dependence of the reversed polarization and switching time. By assuming a domain nucleation mechanism of polarization switching and applying a nonequilibrium statistical model to describe the time dependent polarization reversal probability of nanopolar regions, with a critical volume V^*, Vopsaroiu *et al.* [41] were able to solve these deficiencies and fully reproduce the KAI equations. However, unlike the KAI model, this approach successfully accounted for the applied electric field, time, and temperature contributions to produce comprehensive analytical relations for the reversed polarization, switching time, switching current, and coercive field [41], but also domain wall velocity, Curie law in ferroelectrics [42], and lattice mismatch strain/stress effects [43]. Given that antiferroelectrics consist of two equally and opposing ferroelectric sublattices, in this paper we examine the physics of polarization dynamics in antiferroelectric materials using the nonequilibrium domain nucleation model of Vopsaroiu *et al.* applied to each ferroelectric sublattice [41].

II. ANTIFERROELECTRIC DOUBLE HYSTERESIS LOOP EXPLAINED

Figure 1 shows a typical antiferroelectric double hysteresis loop. We shall refer to the two ferroelectric sublattices of the antiferroelectric as sublattice A and sublattice B. In this convention, at zero applied electric field, sublattice A has negative polarization $P_A = -P_s$, and sublattice B has positive

*Corresponding author: melvin.vopson@port.ac.uk
†Formerly known as Vopsaroiu.

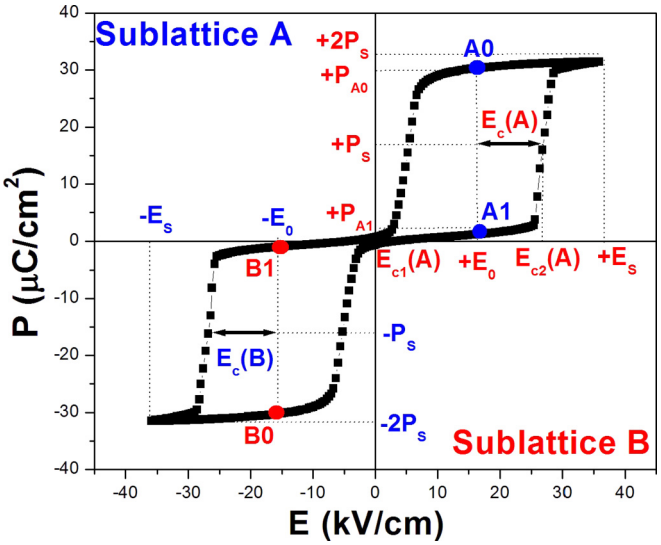

FIG. 1. Typical antiferroelectric double hysteresis loop with the main parameters marked on it.

polarization, $P_B = +P_s$, where P_s is the absolute saturation polarization/spontaneous polarization of each sublattice. Hence, when the applied E field is zero, the antiferroelectric has zero polarization due to the self-cancelation of the macroscopic polarizations of the two consisting ferroelectric sublattices, $P = P_A + P_B = 0$, as seen in Fig. 1. This is also well represented schematically in Fig. 2(a), which shows the zero polarization state and the unit cells of the ferroelectric sublattices A and B, at equilibrium, and under no applied external field. The application of a large enough positive or negative external electric field results in switching of the antiferroelectric from antipolar to polar ferroelectric. Therefore, under the influence of an applied electric field, the antiferroelectric displays a double hysteresis (see Fig. 1), with each hysteresis loop representing the response of the induced ferroelectric phase with polarization in the direction of one of the two sublattices. Hence, a positive applied field, $+E$, would result in the reversal of the negative sublattice A, while leaving the positive sublattice B unaffected [see Figs. 2(d) and 2(e)]. Therefore, the hysteresis loop in the positive quadrant of Fig. 1 corresponds to the reversal of the negative sublattice A. Similarly, a negative applied field, $-E$, would result in the reversal of the positive sublattice B [Figs. 2(b) and 2(c)], and the negative hysteresis loop in Fig. 1 corresponds to the reversal of the positive sublattice B. In order to explain the polarization dynamics of antiferroelectrics and to formulate the theoretical model, we make the following notations on the double hysteresis loop: $E_c(\mathrm{A}) = E_0 - E_{c1}(\mathrm{A}) = E_{c2}(\mathrm{A}) - E_0$ is the coercive field of sublattice A; $E_c(\mathrm{B}) = -E_0 - E_{c1}(\mathrm{B}) = E_{c2}(\mathrm{B}) - E_0$ is the coercive field of sublattice B; $\pm E_s$ are the positive and negative saturation electric fields; $\pm 2P_s$ are the positive and negative saturation polarization values of the whole antiferroelectric sample; $\pm P_s$ are the positive and negative saturation polarization values of each ferroelectric sublattice; $\pm E_0$ are the activation fields at which the hysteresis loops are centered, and they are equivalent to the $E = 0$ axis of

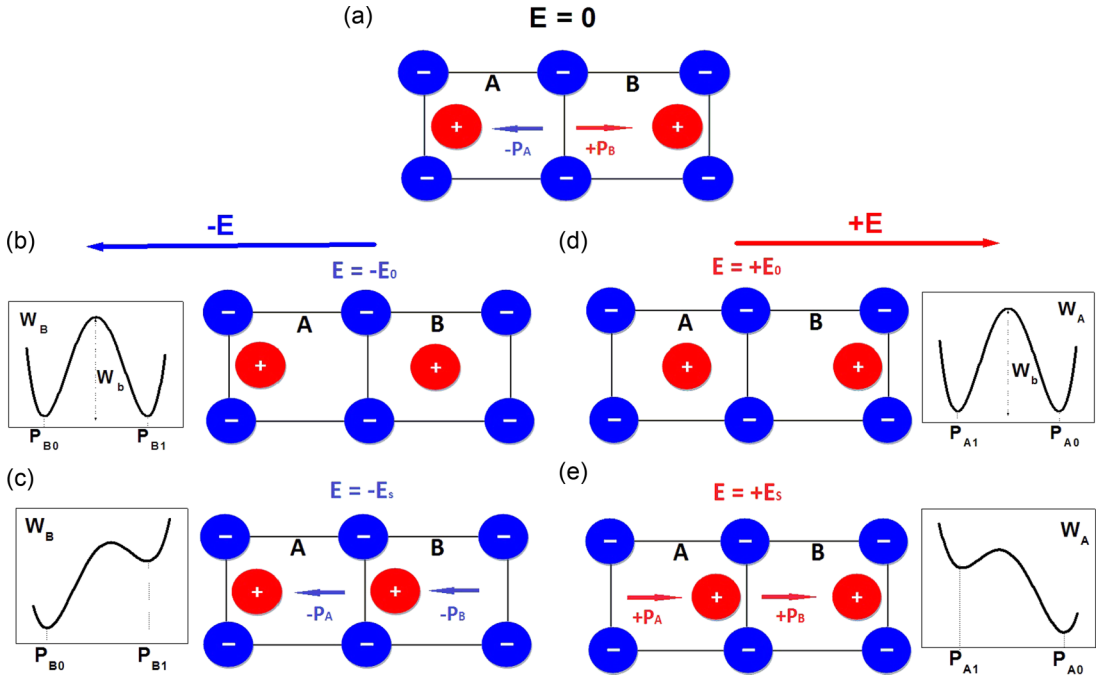

FIG. 2. Schematic diagram of the unit cells of a hypothetical antiferroelectric material consisting of ferroelectric sublattices A and B, respectively. (a) Antiferroelectric in ground state at $E = 0, P = 0$; (b) reversal of the positive sublattice B under the action of negative E field, while sublattice A remains unchanged. At E field equal to the critical activation field, $E = -E_0$, the free energy of sublattice B shows two equally probable energy states corresponding to P_{B0} and P_{B1}. (c) At saturating negative field $E = -Es$, sublattice B is fully reversed; (d) reversal of the negative sublattice A under the action of positive E field, while sublattice B remains unchanged. When $E = +E_0$, the free energy of sublattice A shows two equally probable energy states corresponding to P_{A0} and P_{A1}. (e) When $E = +Es$, the negative sublattice A is fully reversed into positive polarization.

the hysteresis loop of a ferroelectric material; $+E_0$ intersects the positive hysteresis loop of sublattice A at points A0 and A1; and $-E_0$ intersects the negative hysteresis loop of the positive sublattice B at points B0 and B1. The meaning of A0, A1, B0, and B1 is that of pseudoremanent polarization states (see Fig. 1) that can be accessed only when the system is excited at the critical fields $\pm E_0$. $+P_{A0}$ and $+P_{A1}$ are the upper and lower pseudoremanent polarization states of sublattice A, and $-P_{B0}$ and $-P_{B1}$ are the upper and lower pseudoremanent polarization states of sublattice B, respectively (Figs. 1 and 2).

III. THEORY

Having the parameters of the double hysteresis loop defined, we now recall that polar ferroelectric materials display a single hysteresis loop and that they can be described using Landau-Devonshire formalism in terms of their free energy expansion around the order parameter. The free energy function has two equilibrium minima corresponding to the two possible remanent polarization states of a ferroelectric system, separated by an energy barrier, W_b. At $E = 0$, the two possible states are equally probable, and reversal from one state to another can take place only if an energy comparable to W_b is supplied to the system. An applied E field will distort the balance of probabilities and will promote the reversal into one of the two states, depending on the polarity of the applied E field. This is the correct description of the polarization reversal process at $T = 0$ K. If $T \neq 0$ K, then an additional Boltzmann energy term, k_BT, will contribute to the reversal process. In fact, at $T \neq 0$ K, there is a nonzero probability that reversal over W_b occurs even at $E = 0$, leading to spontaneous polarization reversal. The ferroelectric is essentially a nonequilibrium system in which nucleation polar sites undergo statistical transitions between the two physically permitted states on a continuous basis, and the occupation probabilities $\wp_1$ and $\wp_2$ of two possible states are also time dependent (throughout the paper, $\wp$ refers to occupation probability and P refers to electric polarization). The time evolution of the probabilities when a nonequilibrium system goes through different possible states is described by the general Pauli-Master equation [44]:

$$\frac{d\wp_l}{dt} = \sum_{m \neq l} (a_{l,m}\wp_m(t) - a_{m,l}\wp_l(t)), \tag{1}$$

where $1 \leqslant l, m \leqslant \Omega$ with l and m taking integer values and Ω being the number of possible states of the system compatible with the macrostate; $\wp_l(t)$ and $\wp_m(t)$ are the probabilities that the system is in the state l or m at the time t, respectively; $a_{l,m}$ and $a_{m,l}$ are the transition rates per unit time from the state m to state l and vice versa, respectively. For a system in contact with a temperature reservoir, T, the pseudosymmetry relation between the transition rates is

$$a_{l,m}e^{-(W_m/k_BT)} = a_{m,l}e^{-(W_l/k_BT)} = \upsilon_0, \tag{2}$$

where W_m and W_l are the energies in the state m and l, respectively, and υ_0 is a constant equal to the total number of trials per second to overcome the energy barrier, taken as the frequency of the optical phonons in the crystal $\sim 10^{13}$ Hz [38]. Since ferroelectrics are systems with two energy minima states, Eq. (1) has been solved for $\Omega = 2$ (i.e., a two state system) for which $l,m = 1,2$ [41,42]. In the case of antiferroelectrics, the occurrence of the double hysteresis loop implies that there are two metastable equilibrium states for each ferroelectric sublattice, with a total of four metastable equilibrium states corresponding to points A0, A1, B0, and B1, respectively (Fig. 1). This corresponds to $\Omega = 4$ in Eq. (1), while the polarization values of these four metastable states are P_{A0}, P_{A1}, P_{B0}, and P_{B1}, respectively, having the meaning of pseudoremanent polarizations that occur at the critical activation fields $\pm E_0$. Assuming noninteracting nucleation nanopolar sites within each ferroelectric sublattice, then we can apply the nonequilibrium domain nucleation model of Vopsaroiu *et al.* [41] to each ferroelectric sublattice so that instead of $\Omega = 4$ in Eq. (1) resulting in a system of four differential equations, the problem can be solved as two independent systems of two differential equations, corresponding to $\Omega_A = 2$ and $\Omega_B = 2$, respectively. We now refer to Fig. 2 where the free energy of each sublattice at $\pm E_0$ and $\pm E_s$ has been plotted as a function of the polarization of each sublattice. The energy of states A0 and A1 within sublattice A are

$$\begin{aligned} W_{A0} &= -W_b + P_{A0} \times (E - E_0) \\ W_{A1} &= -W_b + P_{A1} \times (E - E_0). \end{aligned} \tag{3}$$

It can be easily noticed that if the applied electric field $E = +E_0$, then $W_{A0} = W_{A1} = -W_b$, as seen in Fig. 2(d). Similarly, the energy of states B0 and B1 within sublattice B are

$$\begin{aligned} W_{B0} &= -W_b + P_{B0} \times (E + E_0) \\ W_{B1} &= -W_b + P_{B1} \times (E + E_0). \end{aligned} \tag{4}$$

Hence, if the applied electric field $E = -E_0$, then $W_{B0} = W_{B1} = -W_b$, as seen in Fig. 2(b). Hence, at $E = +/-E_0$, the two states A0, A1 and B0, B1 are equally probable. Let $\wp_{A0}(t)$ and $\wp_{A1}(t)$ be the probabilities that sublattice A is at time t in state A0 and A1 and that $\wp_{B0}(t)$ and $\wp_{B1}(t)$ are the probabilities that sublattice B is at time t in states B0 and B1, respectively. Solving the Pauli-Master [Eq. (1)] for each sublattice requires an identical approach with the exception that the hysteresis loop of sublattice A is centered at $+E_0$ and that the energy of the states A0 and A1 are given by relation (3), while sublattice B has an activation field $-E_0$ and the energy of states B0 and B1 are given by relation (4). In what follows, we are restricting the analysis to sublattice A, bearing in mind that a similar treatment can be applied to sublattice B by properly considering the energy states and the polarity of the activation field. Solutions of the Pauli-Master [Eq. (1)] for sublattice A are

$$\wp_{A0}(t) = e^{-\left(\frac{t}{t_{SW}}\right)} + \wp_{A0}(\infty) \cdot \left(1 - e^{-\left(\frac{t}{t_{SW}}\right)}\right) \tag{5}$$

$$\wp_{A1}(t) = -e^{-\left(\frac{t}{t_{SW}}\right)} + \wp_{A0}(\infty) \cdot \left(e^{\frac{W_{A1}-W_{A0}}{k_BT}} + e^{-\left(\frac{t}{t_{SW}}\right)}\right), \tag{6}$$

where $\wp_{A0}(\infty)$ is the equilibrium probability of state A0 when $t \to \infty$. Using (3) and the normalization condition

$\wp_{A0}(t) + \wp_{A1}(t) = 1$, $\wp_{A0}(\infty)$ becomes

$$\wp_{A0}(\infty) = \left(1 + e^{\frac{W_{A1} - W_{A0}}{k_B T}}\right)^{-1} = \left(1 + e^{\frac{(E-E_0)(P_{A1} - P_{A0})}{k_B T}}\right)^{-1}. \quad (7)$$

t_{sw} is the polarization switching time at an arbitrary applied E field, given by

$$t_{SW} = \frac{1}{\nu_0} \cdot e^{-\left(\frac{W_{A0}}{k_B T}\right)} = \frac{1}{\nu_0} \cdot e^{\frac{W_b - P_{A0}(E-E_0)}{k_B T}}. \quad (8)$$

At the coercive field of sublattice A, $E_c(A) = E_0 - E_{c1}(A) = E_{c2}(A) - E_0$ (see Fig. 1), the occupation probabilities of states A0 and A1 are equal because the polarization of sublattice A is zero ($P_A = 0$) and the polarization of the whole antiferroelectric sample is $P = P_A + P_B = +P_s$ (see Figs. 1 and 2). This implies that when $E = E_c(A)$, then $\wp_{A0}(t) = \wp_{A1}(t)$ and since $\wp_{A0}(t) + \wp_{A1}(t) = 1$, we deduce that $\wp_{A0}(t) = \wp_{A1}(t) = 0.5$ at the coercive field. Using this condition in (5) and (8) and imposing $\wp_{A0}(\infty) \to 0$ at $E \geqslant E_c(A)$, after some algebraic rearrangement we obtain the coercive field of sublattice A as

$$E_{c2}(\mathrm{A}) = E_0 + \frac{W_b}{2P_s} - \frac{k_B T}{V^* 2P_s} \cdot \ln\left(\frac{\upsilon_o t}{\ln(2)}\right) \quad (9)$$

V^* is the volume of the polar embryo, and it comes from the fact that the energies expressed in (2)–(8) are in fact energies per unit volume. Since the equations refer to the total energy, all energy terms must be multiplied with V^*, which has been omitted for convenience. Similarly, the coercive field of sublattice B is derived as

$$E_{c2}(\mathrm{B}) = -E_0 - \frac{W_b}{2P_s} + \frac{k_B T}{V^* 2P_s} \cdot \ln\left(\frac{\upsilon_o t}{\ln(2)}\right). \quad (10)$$

Equations (9) and (10), describing the coercive fields of sublattices A and B, respectively, as a function of the applied electric field, temperature, time, and activation energy barrier of the nucleation process, allow quick testing of the proposed model against experimental data extracted from polarization hysteresis loops.

It is important to mention that in this approach there is no need to specify the form of the Landau-Devonshire free energy, as all contributions and interactions are captured in the energy barrier term, W_b. In fact, any additional energy terms could be specifically considered in the Landau-Devonshire free energy, including depolarizing energy [41] or interfacial stress/strain [43], without compromising this approach. However, it is widely accepted that the depolarizing fields are only significant in thin film structures and negligible in bulk [45], especially bulk antiferroelectrics, as in this paper. Hence, the present approach neither requires the inclusion of these effects, nor are they relevant for the current paper. In this nonequilibrium statistical approach, we also do not specify the exact location of the nucleation sites, which could be at special sites where the presence of defects or residual antiparallel domains could lower the activation energy barrier. Although beyond the scope of this paper, in future studies, a more detailed approach could incorporate these effects as well as additional local fields, distribution of fields, distribution of volumes of the nucleation sites, and other energy terms in order to extract additional information from the measurements.

IV. EXPERIMENTS AND RESULTS

To test the model a ceramic antiferroelectric sample $Pb_{0.99}Nb_{0.02}[(Zr_{0.57}Sn_{0.43})_{1-y}Ti_y]_{0.98}O_3$ with $y = 0.06$ (code name PNZST 43/6/2) has been synthesized. Powders of PbO, ZrO_2, SnO_2, TiO_2, and Nb_2O_5 with purity levels >99.9% were batched with an additional 5 wt.% PbO to compensate for PbO evaporation during calcination and sintering. Calcination was repeated twice at 935°C for 4 h for compositional homogeneity. The powder was milled for 7 h in ethanol with zirconia media, dried, and pressed. After a final milling of 15 h, 40 g of dried PNZST 43/6/2 powder with acrylic binder was pressed at 75 MPa. Cold isostatic pressing was then applied to the green compact at 400 MPa. After the binder was burnt out at 450°C, sintering was carried out at 1325°C for 3 h. To further increase the density of the ceramic, hot isostatic pressing was carried out at 1150°C and 200 MPa for 2 h in a 20%O_2, 80% Ar atmosphere. Transmission electron microscopy (TEM) was used to analyze the microstructure of the as-processed ceramic. The TEM specimens were prepared via mechanical dimpling and an argon ion mill. Domain morphology and incommensurate modulations were imaged with a Phillips CM-30 transmission electron microscope operating at 300 kV. Polarization hysteresis loops were acquired using an aixACCT Piezo-Test Analyzer 2000E, which was equipped with a sample heating stage and temperature controller in order to perform sample measurements as a function of temperature. The sample used for the polarization measurement is a ceramic disk of 10 mm diameter and 500 μm thickness with metallic electrodes applied on each side of the ceramic disk. Hysteresis loops were acquired using a triangular field waveform of frequency 0.1 Hz and 1.8 kV amplitude with a prepolarization pulse applied first. Due to the large applied voltages, measurements were only possible at low <1 Hz frequencies. We observed no significant changes in the double hysteresis loops when measurements were taken at 0.05, 0.1, 0.2, and 0.5 Hz, respectively. The switching current range was 1 mA for this particular sample and experimental conditions. Figure 3 shows the double hysteresis loops measured at room temperature and

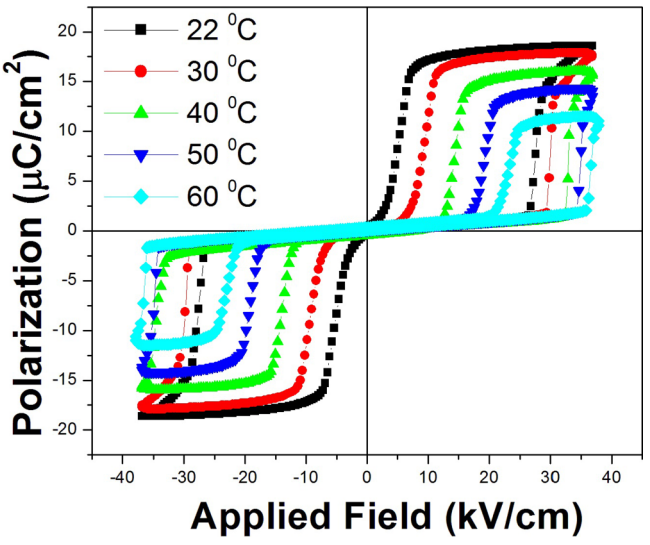

FIG. 3. Polarization hysteresis loops as a function of temperature for PNZST 43/6/2 antiferroelectric sample.

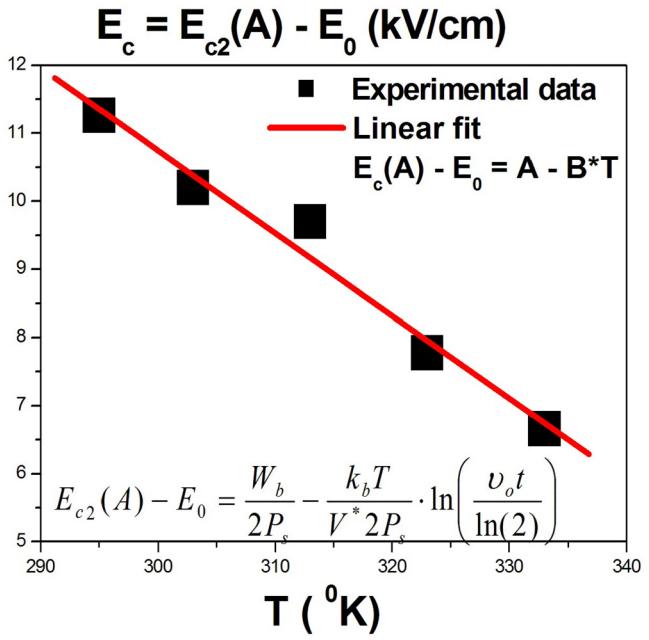

FIG. 4. Experimental and theoretical fit of the coercive field values of sublattice A as a function of temperature. The theoretical Eq. (9) has been used to fit the experimental data.

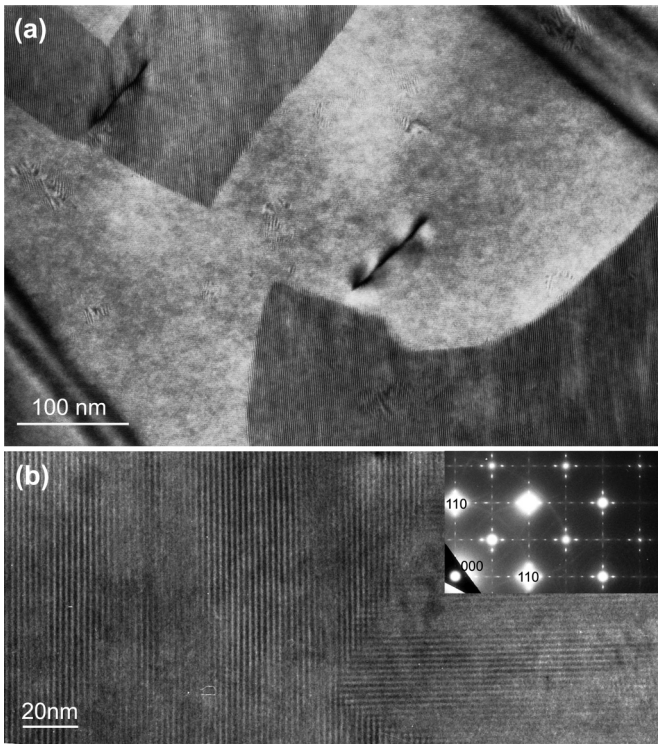

FIG. 5. Representative microstructure in the PNZST 43/6/2 ceramic. (a) The antiferroelectric 90° domains; (b) the thin 180° domain slabs. The inset in (b) displays the corresponding selected area electron diffraction pattern.

elevated temperatures ranging from 22°C to 60°C. Although our system allows testing up to 600°C, measurements at higher temperatures were not possible because of multiple cracks and physical sample damage emerging at temperatures above 60°C. From the double hysteresis loop at room temperature, we extracted the following parameters of the PNZST 43/6/2 antiferroelectric sample: $2P_s = 37.4\,\mu\text{C/cm}^2$, $P_\text{A} = |P_\text{B}| = P_s = 18.7\,\mu\text{C/cm}^2$, $\pm E_0 = 16.6\,\text{kV/cm}$, and $\pm E_s = 36\,\text{kV/cm}$. The electric coercive field was extracted by averaging the $E_c(\text{A})$ from relations $E_c(\text{A}) = E_0 - E_{c1}(\text{A})$ and $E_c(\text{A}) = E_{c2}(\text{A}) - E_0$ for sublattice A. The same values, but with an opposite sign, are obtained for the coercive field of sublattice B. Figure 4 shows the dependence of the experimental $E_c(\text{A})$ values on the measurement temperature. Equation (9) predicts that $E_c(\text{A})$ has a theoretical maximum value at $T = 0\,\text{K}$, and then it decreases linearly with a negative slope as the temperature increases. Remarkably, this is exactly what has been observed experimentally, which has enabled us to perform a theoretical fit to the experimental data using Eq. (9). The theoretical fit using the linear function $E_c(\text{A}) = \text{A} - B \times T$, resulted in $\text{A} = 47.11\,\text{kV/cm}$ and $\text{B} = 0.121\,\text{kV/cm K}$ fitting values. Combining (9) with the linear fitting results, we obtain by identification $\text{B} = \frac{k_B}{V^* 2P_s} \cdot \ln(\frac{\upsilon_o t}{\ln(2)})$.

The meaning of t is the fraction of the measurement time taken from the saturating applied electric field to the coercive field. Since the measurements are performed at 0.1 Hz, then the measurement time for the whole double hysteresis loop is 10 s, which is split in 5 s per sublattice hysteresis loop. Hence, the estimated time is $t = 2.5\,\text{s}$. Taking $\upsilon_0 = 10^{13}\,\text{Hz}$, $k_B = 1.38 \times 10^{-23}\text{J/K}$, $2P_s = 37.4\,\mu\text{C/cm}^2$, and $\text{B} = 0.121\,\text{kV/cm K}$ from the fitting, we determined the volume of the nucleation nanopolar region to be $V^* = 98 \times 10^{-27}\,\text{m}^3$. This corresponds to a linear length scale of 2.86 nm for the polar phase. Similarly, the intercept $A = W_b/2P_\text{s} = 47.11\,\text{kV/cm}$ allowed us to calculate the energy barrier $W_b = 2P_\text{s} \times A \times V^* = 1.07\,\text{eV}$. The meaning of this energy barrier is the activation energy of the polarization reversal of the ferroelectric sublattice at the activation $\pm E_0$ field.

The theoretically estimated critical size of the polar phase is in good agreement with the microstructure analysis of the PNZST 43/6/2 ceramic. Figure 5 displays the typical domain morphology and incommensurate modulations in a grain imaged along the [001] zone axis. According to previous studies [46], the patches in Fig. 5(a) are antiferroelectric 90° domains. Within each 90° domain are the thin 180° domains, which appear as fringes in bright-field images. Figure 5(b) shows these fringes across a 90° domain wall where vertical fringes are seen in the left part of the micrograph and horizontal fringes are seen in the lower right part. The corresponding selected area diffraction pattern in the inset shows satellite diffraction spots with an incommensurate number of 7.20 [46]. This indicates a wavelength of 2.09 nm, consistent with the fringe spacing directly measured from the bright-field micrograph. According to our previous model for antiferroelectric domains [46], the average thickness of the 180° domain slabs is then around 1 nm. Therefore, the theoretically estimated critical size of ~2.8 nm is very reasonable. Once one or two slabs of 180° domains are reversed, the critical size is reached, and the polar phase can grow further under applied electric field. The coexistence of antiferroelectric and ferroelectric domains are clearly identified in the TEM bright field micrographs of antiferroelectric PNZST 43/6/2.

V. CONCLUSIONS

A domain nucleation nonequilibrium statistical model has been applied to explain the polarization dynamics of antiferroelectric materials. A suitable antiferroelectric $Pb_{0.99}Nb_{0.02}[(Zr_{0.57}Sn_{0.43})_{0.94}Ti_{0.06}]_{0.98}O_3$ ceramic sample has been fabricated, which allowed experimental confirmation of the model's theoretical predictions. The model and the experimental evidence suggest that polarization reversal in antiferroelectrics takes place via a domain nucleation process within each ferroelectric sublattice. The process is triggered in nucleation sites by forming nanometer-sized polar phase. Using the theoretical model together with the experimental data, we calculated the average volume of the nucleation polar phase to be $V^* = 98 \times 10^{-27}\text{m}^3$. This is equivalent to a linear length scale of 2.86 nm. We also determined that the energy barrier of the nucleation polar phase polarization reversal within each sublattice is $W_b = 1.07$ eV at the activation field $\pm E_0$. These results advance our understanding of antiferroelectrics, a class of increasingly important materials, and facilitate their adequate theoretical modelling, fabrication, and applications design.

ACKNOWLEDGMENTS

MV acknowledges that the equipment used in this paper was funded by the University of Portsmouth, Faculty of Science, and XT would like to acknowledge that this paper was supported by the National Science Foundation (NSF) through Grant No. DMR-1465254.

[1] C. Kittel, Phys. Rev. **82**, 729 (1951).
[2] G. Shirane, Phys. Rev. **86**, 219 (1952).
[3] E. Sawaguchi, J. Phys. Soc. Jpn. **8**, 615 (1953).
[4] X. Tan, S. E. Young, Y. H. Seo, J. Y. Zhang, W. Hong, and K. G. Webber, Acta Mater. **62**, 114 (2014).
[5] X. Hao, Y. Wang, L. Zhang, L. Zhang, and S. An, Appl. Phys. Lett. **102**, 163903 (2013).
[6] M. S. Mirshekarloo, K. Yao, and T. Sritharan, Appl. Phys. Lett. **97**, 142902 (2010).
[7] A. Chauhan, S. Patel, R. Vaish, and C. R. Bowen, Materials **8**, 8009 (2015).
[8] J. Ge, D. Remiens, X. Dong, Y. Chen, J. Costecalde, F. Gao, F. Cao, and G. Wang, Appl. Phys. Lett. **105**, 112908 (2014).
[9] A. S. Mischenko, Q. Zhang, J. F. Scott, R. W. Whatmore, and N. D. Mathur, Science **311**, 1270 (2006).
[10] S. T. Zhang, A. B. Kounga, W. Jo, C. Jamin, K. Seifert, T. Granzow, J. Rödel, and D. Damjanovic, Adv. Mater. **21**, 4716 (2009).
[11] A. P. Tomas, M. L. Cnatu, and G. Catalan, Adv. Mater. **28**, 9644 (2016).
[12] M. M. Vopson, G. Caruntu, and X. Tan, Scr. Mater. **128**, 61 (2017).
[13] M. Pešic, M. Hoffmann, C. Richter, T. Mikolajick, and U. Schroeder, Adv. Funct. Mater. **26**, 7486 (2016).
[14] M. M. Vopson and X. Tan, IEEE Electron Device Lett. **37**, 1151 (2016).
[15] H. Ishiwara, J. Nanosci. Nanotechnol. **12**, 7619 (2012).
[16] A. Sheikholeslami and P. G. Gulak, Proc. IEEE **88**, 667 (2000).
[17] J. F. Scott, Struct. Bond. **124**, 199 (2007).
[18] R. Guo, L. You, Y. Zhou, Z. S. Lim, X. Zou, L. Chen, R. Ramesh, and J. Wang, Nat. Commun. **4**, 1990 (2013).
[19] Y. Kato, Y. Kaneko, H. Tanaka, K. Kaibara, S. Koyama, K. Isogai, T. Yamada, and Y. Shimada, Jpn. J. Appl. Phys. **46**, 2157 (2007).
[20] A. K. Tagantsev, K. Vaideeswaran, S. B. Vakhrushev, A. V. Filimonov, R. G. Burkovsky, A. Shaganov, D. Andronikova, A. I. Rudskoy, A. Q. R. Baron, H. Uchiyama, D. Chernyshov, A. Bosak, Z. Ujma, K. Roleder, A. Majchrowski, J.-H. Ko, and N. Setter, Nat. Commun. **4**, 2229 (2013).
[21] X. Hao, J. Zhai, L. B. Kong, and Z. Xu, Prog. Mater. Sci. **63**, 1 (2014).
[22] H. Guo and X. Tan, Phys. Rev. B **91**, 144104 (2015).
[23] I. B. Misirlioglu, L. Pintilie, K. Boldyreva, M. Alexe, and D. Hesse, Appl. Phys. Lett. **91**, 202905 (2007).
[24] W. J. Merz, Phys. Rev. **95**, 690 (1954).
[25] D. Berlincourt and H. A. Krueger, J. Appl. Phys. **30**, 1804 (1959).
[26] D. Damjanovic, Rep. Prog. Phys. **61**, 1267 (1998).
[27] R. Landauer, J. Appl. Phys. **28**, 227 (1957).
[28] A.-Q. Jian, H. J. Lee, C. S. Hwang, and T.-A. Tang, Phys. Rev. B **80**, 024119 (2009).
[29] L. Tian, D. A. Scrymgeour, and V. Gopalan, J. Appl. Phys. **97**, 114111 (2005).
[30] S. Hashimoto, H. Orihara, and Y. Ishibashi, J. Phys. Soc. Jpn. **63**, 1601 (1994).
[31] H. Orihara, S. Hashimoto, and Y. Ishibashi, J. Phys. Soc. Jpn. **63**, 1031 (1994).
[32] A. N. Kolmogorov, Izv. Akad. Nauk. Ser. Math. **3**, 355 (1937).
[33] M. Avrami, J. Chem. Phys. **8**, 212 (1940).
[34] V. Shur, E. Rumyantsev, and S. Makarov, J. Appl. Phys. **84**, 445 (1998).
[35] V. Shur and E. Rumyantsev, Ferroelectrics **151**, 171 (1994).
[36] A. K. Tagantsev, I. Stolichnov, N. Setter, J. S. Cross, and M. Tsukada, Phys. Rev. B **66**, 214109 (2002).
[37] O. Lohse, M. Grossmann, U. Boettger, D. Bolten, and R. Waser, J. Appl. Phys. **89**, 2332 (2001).
[38] X. J. Lou, J. Phys.: Condens. Matter **21**, 012207 (2009).
[39] Y. W. So, D. J. Kim, T. W. Noh, Jong-Gul Yoon, and T. K. Song, Appl. Phys. Lett. **86**, 092905 (2005).
[40] J. Y. Jo, H. S. Han, J. G. Yoon, T. K. Song, S. H. Kim, and T. W. Noh, Phys. Rev. Lett. **99**, 267602 (2007).
[41] M. Vopsaroiu, J. Blackburn, M. G. Cain, and P. M. Weaver, Phys. Rev. B **82**, 024109 (2010).
[42] M. Vopsaroiu, P. M. Weaver, M. G. Cain, M. J. Reece, and K. B. Chong, IEEE Trans. Ultrason. Ferroelectr. Freq. Control **58**, 1867 (2011).
[43] Y. Zhang, X. L. Zhong, M. Vopson, J. B. Wang, and Y. C. Zhou, J. Appl. Phys. **112**, 014112 (2012).
[44] H. J. Kreuzer, *Nonequilibrium Thermodynamics and Its Statistical Foundations* (Oxford University Press, Oxford, 1981) Ch. 10.
[45] M. D. Glinchuka, E. A. Eliseeva, and V. A. Stephanovich, Physica B **322**, 356 (2002).
[46] H. He and X. Tan, Phys. Rev. B **72**, 024102 (2005).